

# Auto4D: Learning to Label 4D Objects from Sequential Point Clouds

Bin Yang<sup>1,2</sup> Min Bai<sup>1,2</sup> Ming Liang<sup>1</sup> Wenyuan Zeng<sup>1,2</sup> Raquel Urtasun<sup>1,2</sup>

<sup>1</sup>Uber Advanced Technologies Group <sup>2</sup>University of Toronto

{byang10, mbai3, ming.liang, wenyuan, urtasun}@uber.com

## Abstract

*In the past few years we have seen great advances in 3D object detection thanks to deep learning methods. However, they typically rely on large amounts of high-quality labels to achieve good performance, which often require time-consuming and expensive work by human annotators. To address this we propose an automatic annotation pipeline that generates accurate object trajectories in 3D (i.e., 4D labels) from LiDAR point clouds. Different from previous works that consider single frames at a time, our approach directly operates on sequential point clouds to combine richer object observations. The key idea is to decompose the 4D label into two parts: the 3D size of the object, and its motion path describing the evolution of the object’s pose through time. More specifically, given a noisy but easy-to-get object track as initialization, our model first estimates the object size from temporally aggregated observations, and then refines its motion path by considering both frame-wise observations as well as temporal motion cues. We validate the proposed method on a large-scale driving dataset and show that our approach achieves significant improvements over the baselines. We also showcase the benefits of our approach under the annotator-in-the-loop setting.*

## 1. Introduction

Self-driving vehicles have the potential to revolutionize transportation. One of the key ingredients of any autonomy system is the ability to perceive the scene and predict how it might unroll in the near future. This is important for the subsequent motion planner to plan a safe and comfortable maneuver towards its goal. In recent years, we have seen tremendous advances in 3D perception and motion forecasting [30, 12, 41, 40, 6, 3] thanks to the adoption of deep learning. However, deep learning-based approaches require massive amounts of labelled data. In the context of perception and motion forecasting, annotations are required in the form of accurate 3D bounding boxes over time. We refer to these space-time bounding box annotations as 4D labels.

Unlike annotations in the image domain, creation of 3D

bounding box labels using LiDAR points is a complex task due to the sparsity of the observations. The exact extent, size, and pose of an object are often unclear from a single observation. Therefore, human annotators must “detect” each object in each frame while considering the additional evidence over the trajectory sequence to help accurately estimate the size and location of each object. This is exacerbated by the ambiguity in visualizing 3D information on a 2D display for the annotator and retrieve 3D input. This process is extremely tedious, time consuming and expensive. For example, more than 10 hours are required to accurately annotate a 25 seconds scene at 10Hz. As such, there is tremendous value in automating label creation or in creating human-in-the-loop refinement systems that correct labels that have been created automatically.

In recent years, researchers have proposed numerous works for object detection [30, 12, 41, 40, 38, 25]. However, most of these works use only data from a single timestep or past measurements from a very short history. A number of works further target the task of associating detections over time as object tracks [20, 36]. However, these techniques produce bounding boxes that are often not consistent over time in size and often do not construct a smooth, accurate, and realistic trajectory. On the other hand, some existing work have attempted to perform bounding 3D bounding box refinement over time by considering the entire trajectory. For example, [26] pioneered the inclusion of handcrafted 3D motion priors to refine detections. [33] attempts to generate automatic 4D annotations by focusing on only static vehicles. However, because of their limitations in motion modeling capability or scenarios targeted, their application in automatic label generation is limited.

Instead, we propose an auto-labeling model that holistically considers the LiDAR points collected over the entire trajectory of an object. In particular, we focus on the 4D annotation of vehicles, as they are often the most numerous traffic participants in a scene. Our technique is inspired by iterative (semi-) automatic label generation and refinement techniques such as [1]. We first leverage a pipeline built on existing object detection and discrete association as a cheap but noisy initialization to isolate the trajectories of

individual vehicles; we note that this initialization can also come from coarse and fast human annotation. Then, we apply a two-branch network. The first branch is a local object size reasoning model that predicts a single set of bounding box dimensions using the noisy aggregation of LiDAR points over the entire trajectory. The second branch consists of a global trajectory refinement model which exploits the size estimate from the first branch and employs a spatial-temporal encoder-decoder to refine the path of the vehicle.

We demonstrate the effectiveness of our model on a novel large-scale driving dataset with annotations of much higher quality than available datasets. Existing datasets either have a limited number of object trajectories [11], or make a compromise in the label quality with sparse annotation and linear interpolation [2]. Compared with the noisy initialization, we show that our model can improve the number of precise bounding boxes (with IoU greater than 0.9) by 36%, while the baseline using offline detection and tracking only brings a relative gain of less than 2%. In addition, we also demonstrate our model’s ability to iteratively improve label quality in the annotator-in-the-loop setting.

## 2. Related Work

**3D Object Detection:** With the growing interest in autonomous driving, a large number of works have targeted 3D object detection in recent years. Many techniques operate on LiDAR points as input. Due to the sparsity and unordered nature of the point clouds, some techniques rasterize the points into a perspective view representation [25, 19, 7] and leverage well developed detection schemes for images. To better preserve the 3D distances in the scene, a different line of work discretizes the points into voxels and computes various types of handcrafted [8, 18, 30] or learned features [44] before applying 3D convolutions. An increasingly popular alternative [23, 39, 16, 38] operate in bird’s eye view by encoding the height dimension as a feature for efficient computation. Finally, a number of works propose to directly operate on the point structures [41, 27, 31]. However, these methods exploit only the information captured by the sensors at a single instant, or aggregate information over a very short (0.5s) duration [40, 42].

In our setting we target the offline bounding box generation task, where we can leverage temporal information over a much longer period to improve the bounding box quality.

**Temporal Object Detection and Tracking:** Given a sequence of observations as input, techniques have been proposed to use information over time to increase accuracy of detections at each instant. In the case of images, learned flow is often used to propagate information across frames via warping, upon which the aggregated features are used for more accurate detection [45, 35]. Other works propagate information between frames implicitly without com-

puting flow [9]. In these works, the typically smooth deformations of the bounding box and its location are implicitly learned and serve to improve the detections. However, due to the perspective transformation in image space, learning priors for the deformations is complicated. Other works incorporate priors in 3D space, often using handcrafted costs as part of an energy minimization framework [26]. A relatively recent technique [10] uses implicit memory of the 3D scene to exploit temporal clues while also being efficient. Finally, techniques leveraging deep learning to refine frame-wise object detections using temporal information and 3D motion have been proposed [13, 20]. In contrast with these techniques, we consider an extended sequence of input data at the same time, while also strictly enforcing a constant size constraint that applies to 3D bounding boxes of non-deformable objects such as vehicles.

**(Semi-) Automatic Labeling:** Given the expense of creating human annotated datasets, a number of works have targeted automatic or user-in-the-loop semi-automatic label generation. In the setting of creating 3D bounding box labels, [24, 17] learn to predict the 3D cuboid from the nearby points around the center with a fixed neighborhood size (*i.e.*, object size prior). [34] reasons about the cuboid during the first frame given one-click annotation, and then applies a Kalman filter based object tracker to generate the labels in the following trajectory. In contrast, our refinement technique can be initialized using either human input or imperfect detections from off-the-shelf detectors. [43] proposed an interesting technique that leverages differentiable 3D shape decoding and rendering to iteratively fit detailed 3D vehicle shapes to observed image and LiDAR evidence to generate automatic 3D labels, but only makes use of single frames, unlike our model. Finally, [33] restricts its domain to only consider detector-generated bounding boxes of static vehicles and generate a final label using the weighted sum of all associated detections. On the other hand, our work is able to seamlessly handle both dynamic and static objects through its flexible motion modeling. In a related realm, works such as [5, 1, 22] which target automatic labels in the image domain demonstrate both the possibility and value in combining human abilities with deep learning to greatly accelerate label generation. We note that our technique is likewise able to refine coarse initial annotations as well as detections from preprocessing to achieve greater label accuracy.

## 3. Learning to Label 4D Objects

We propose Auto4D, a new automatic labeling approach that recovers 3D object trajectories from sequential point clouds in the context of self-driving. While previous methods [43, 5] mostly focus on single-frame object labels either in 2D or 3D, in this paper we aim to generate temporally

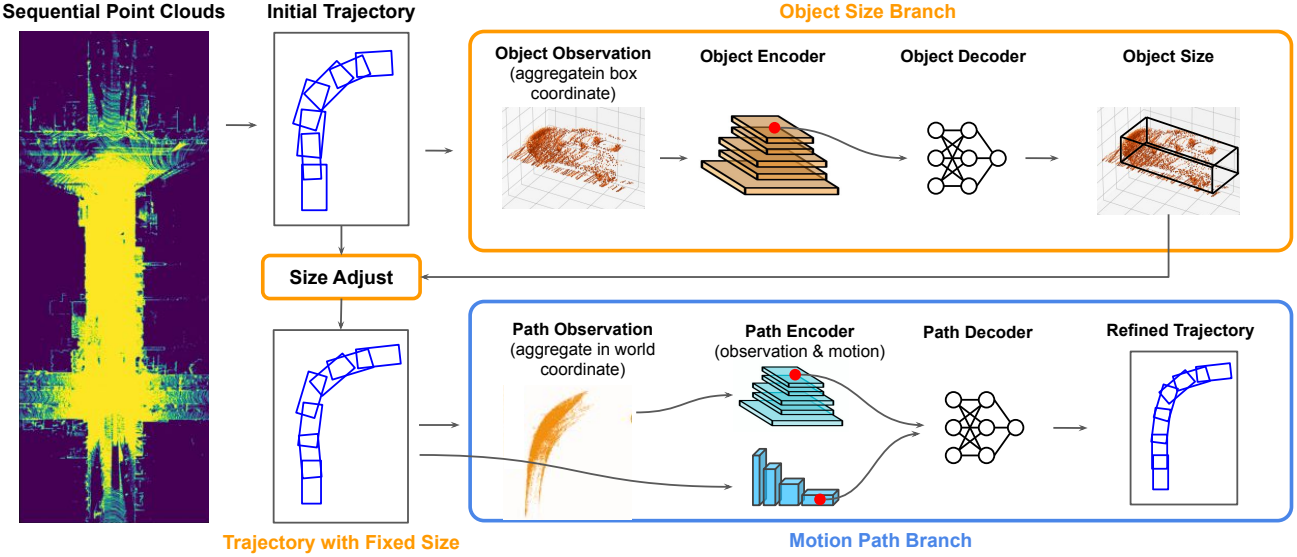


Figure 1. Architecture overview of the proposed model that recovers 4D object labels from sequential point clouds.

consistent object labels in 3D space (dubbed 4D labels). As vehicles comprise a large portion of dynamic traffic participants in a scene, we focus on the automatic annotation of this class in our work. Note that we can easily extend this work to cover other classes such as pedestrians and bicycles. An overview of the proposed method is shown in Figure 1. For detailed network architectures and implementation details we refer the readers to the supplementary material. In this section, we first define the problem we are solving by introducing the input and output representations. We then explain in turn how we reason about the permanent attribute – size, and the transient attribute – pose (or motion path). Lastly we provide details of the model’s training and inference.

### 3.1. Input and Output Representations

Our method, named Auto4D, takes as input 3D measurements across time of a scene captured by a LiDAR sensor on top of a self-driving vehicle. Additionally, we use a pre-trained off-the-shelf 3D object detector and tracker to generate the initial object trajectories. Auto4D then processes each object trajectory individually, and produces a fixed object size prediction along with a refined motion path.

In particular, we take the point clouds captured over all the LiDAR sweeps to form the observation  $\mathbf{x} \in \mathcal{X}$ , where  $\mathbf{x}$  denotes a set of 4D points (3D position + time). We represent these points in the world coordinate system instead of the sensor coordinate system so that we can reason about the object motion independent of the movement of the ego car.

Auto4D extracts object trajectories from the observations in the same world coordinate system. We represent the objects to be labeled with a 2D bounding box in the bird-

eye-view (BEV) space. This representation is selected as the typical downstream modules in self-driving (such as the motion planner) reasons in the same BEV space. We first obtain initial object trajectories by applying a pre-trained off-the-shelf 3D object detector followed with a discrete tracker. In particular, we use a voxel based object detector following KITTI state-of-the-art [38], and a multi-object 3D tracker following [37]. As a result, each object trajectory is composed of a set of detections  $\mathbf{O} = \{\mathbf{D}_i\}$  where  $i$  indexes the frame in which the object is observed.

Each detection  $\mathbf{D}_i = (\mathbf{p}, \mathbf{s}, t)$  consists of three parts: the detection timestamp  $t$ , the object pose  $\mathbf{p} = (x, y, \theta)$  indicating the center position and orientation at timestamp  $t$ , and the object size  $\mathbf{s} = (w, l)$ . Note that the 3D detector and tracker we used does not exploit the assumption that the object size should be constant. Therefore, the initial estimations for the object’s size may vary over the trajectory.

While the initial object trajectory  $\mathbf{O}$  is produced in the online setting, our method refines it in the offline setting given the full observation  $\mathbf{x}$ . Our model consists of a box branch which reasons about the object size in object coordinate system, and a path branch which refines the object center locations along the trajectory in the world coordinate system. Below we explain these two branches in turn.

### 3.2. Box Branch: Permanent Size

The box branch aggregates partial observations of the object at different timestamps in the box coordinate using the bounding boxes provided by the initialization, and produces a single bounding box size for the entire trajectory. Over the course of the trajectory, the relative motion between the ego-vehicle and the object allows for observations of the same object from different viewpoints, thus creating

a denser and more complete point cloud. This richer information allows our model to produce object size estimates with higher accuracy than online detectors that use single (or a small number of) sweeps.

**Object Observation:** Given the sequential point cloud data  $\mathbf{x}$  and initial object trajectory  $\mathbf{O}$  we construct a dense point cloud by aggregating the object’s LiDAR point clouds. Specifically, for each detection  $\mathbf{D} = (\mathbf{p}, \mathbf{s}, t)$ , we extract points inside the bounding box defined by  $\mathbf{D}$  from the corresponding LiDAR sweep. To tolerate detection noise, we scale the bounding box size  $\mathbf{s} = (w, l)$  by  $1.1 \times$  when extracting interior points. We then transform these detection-specific points from world coordinates to object coordinates and aggregate these partial observations across all timestamps. The resulting object observation  $\mathbf{x}_{\text{box}}^{\mathbf{O}}$  can be considered as a *noisy* shape reconstruction of the object, where the noise comes from the errors in the initialization motion path and bounding box size.

**Object Encoder:** The object encoder is used to extract high-resolution spatial features in BEV, which will later be used to reason about the object size. Towards this goal, we project the points in  $\mathbf{x}_{\text{box}}^{\mathbf{O}}$  to the BEV plane and generate the corresponding pseudo-image in BEV. Then, we apply a 2D convolutional network (CNN) to effectively enlarge the receptive field and handle variance in object scale.

$$\mathcal{F}_{\text{object}} = \text{CNN}_{\text{box}}(\mathbf{x}_{\text{box}}^{\mathbf{O}}) \quad (1)$$

To preserve fine-grained details while being efficient in computation, we generate the BEV pseudo-image by voxelizing the point clouds with a voxel size of  $5 \times 5 \text{ cm}^2$ . Note that the time information in  $\mathbf{x}_{\text{box}}^{\mathbf{O}}$  is ignored for the purpose of object size estimation. The output of the object encoder is a 3D feature map  $\mathcal{F}_{\text{object}}$  of size  $C \times H \times W$ , where  $H \times W$  are the BEV dimensions.

**Object Decoder:** Since the receptive field in  $\mathcal{F}_{\text{object}}$  is large enough to cover the whole object, we simply query the feature at object center  $\mathbf{c} = (0, 0)$  from  $\mathcal{F}_{\text{object}}$ , and apply a multi-layer perceptron (MLP) to predict the object size

$$s' = \text{MLP}_{\text{size}}(\mathcal{F}_{\text{object}}(\mathbf{c})) \quad (2)$$

The feature query operator is implemented via bilinear interpolation at object center  $\mathbf{c}$ , *i.e.*, BEV coordinate  $(0, 0)$ .

**Object Size Adjustment:** We update the size of all detections in the object trajectory using the new estimate. One possibility is to update only the width and length of the bounding boxes while retaining the original object center and orientation. However, this may not be a good choice

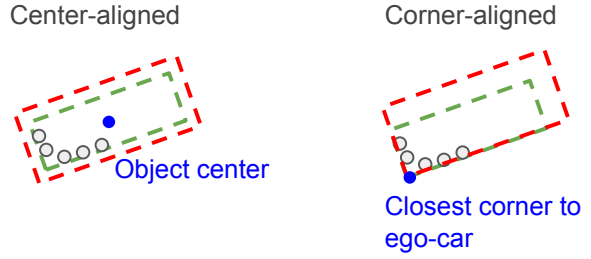


Figure 2. **Two different strategies to adjust object size.** The green box is the original estimate, while the red box is the one with refined object size.

in practice, especially on object detections produced from LiDAR data which have biases in their mistakes. This is the case as 3D point observations of vehicles tend to clearly show a subset of the corners and sides of a vehicle, while others are hidden due to occlusion. To address this, we propose to anchor the newly refined box to the corner closest to the ego-vehicle in the initialization detection which is likely the most clearly visible, and adjust the width and length of the bounding box using our refinement results. In this way, the object center location is also refined, and as a result the object motion path benefits from more accurate object size. We provide a comparison of center-aligned and corner-aligned size adjustment strategies in Figure 2.

### 3.3. Path Branch: Transient Locations

The goal of the path branch is to refine the object’s motion path conditioned on both the aggregated observations in world coordinates as well as the initial motion path (after size adjustment). Relying on the sensor observation helps to better localize the detection at each frame, while exploiting temporal motion information provides additional cues for frames where the object observations are sparse or heavily occluded.

**Path Observation:** We generate the aggregated observation of the full path by extracting points within the object trajectory  $\mathbf{O} = \{\mathbf{D}_i\}$  from the sequential point cloud data  $\mathbf{x}$  to form  $\mathbf{x}_{\text{path}}^{\mathbf{O}}$ . The extraction process is largely identical to that used in the box branch, with the exclusion of the world-to-object coordinate transformation and inclusion of time information in the point clouds. Keeping the 4D points in the world coordinates retains the accurate displacement information for effective motion reasoning.

**Path Encoder:** The path encoder is used to extract fine-grained spatial-temporal features from the 4D point clouds  $\mathbf{x}_{\text{path}}^{\mathbf{O}}$ . We observe that vehicles follow largely smooth trajectories in practice, which provides a strong regularization

to improve object localization at each time step. As a result, we also explicitly encode the motion feature of the path.

Specifically, we generate a 3D voxel grid by consolidating both the height and time dimension as feature channels [4], and apply a 2D CNN to extract multi-scale feature maps:

$$\mathcal{F}_{\text{path}} = \text{CNN}_{\text{path}}(\mathbf{x}_{\text{path}}^{\text{O}}) \quad (3)$$

The output is a 3D feature map  $\mathcal{F}_{\text{path}}$  with the shape of  $C \times H \times W$ , where  $H \times W$  is the BEV dimension, and  $C$  is the channel dimension. To explicitly model motion, we first extract frame-wise motion features for each detection as the pose displacement from the previous frame. For the first frame we manually set its motion features to zero.

$$\mathbf{h}_{\text{motion}}^i = [x^i - x^{i-1}, y^i - y^{i-1}, \theta^i - \theta^{i-1}] \quad (4)$$

We then concatenate these frame-wise motion features along the time dimension and perform temporal feature extraction with a 1D CNN based UNet [28]

$$\mathcal{F}_{\text{motion}} = \text{UNet}_{\text{conv1d}}(\mathbf{h}_{\text{motion}}) \quad (5)$$

**Path Decoder:** We decode the motion path in a convolutional manner. Given the initial detection  $\mathcal{D} = (x, y, \theta, w, l, t)$  along the trajectory, we predict its pose refinement  $\Delta \mathbf{p} = (\Delta x, \Delta y, \Delta \theta)$  taking into account both the LiDAR voxel feature as well as the explicit motion feature:

$$\Delta \mathbf{p} = \text{MLP}_{\text{path}}(\mathcal{F}_{\text{path}}(\mathbf{p}), \mathcal{F}_{\text{motion}}(t)) \quad (6)$$

where  $\mathbf{p} = (x, y)$  is the detection center, and  $t$  is the detection timestamp. The refined pose  $\mathbf{p}' = (x', y', \theta')$  is then computed as follows:

$$x' = (1 + \Delta x) * x \quad (7)$$

$$y' = (1 + \Delta y) * y \quad (8)$$

$$\theta' = \theta + \Delta \theta \quad (9)$$

The feature query  $\mathcal{F}_{\text{path}}(\mathbf{p})$  is implemented as a bilinear interpolation, while the feature query on  $\mathcal{F}_{\text{motion}}$  is simply done by indexing.

### 3.4. Learning and Inference

The proposed model has two outputs: the object’s size from the box branch, and the frame-wise pose from the path branch. Since the path branch depends on the output of the box branch (*i.e.* size adjustment), we train the two branches sequentially. The same loss  $\mathbf{L}(\mathbf{D}, \mathbf{G})$  is applied to both branches, which is defined as the IoU loss between the estimated and ground-truth bounding boxes. Note that when the IoU is zero (*i.e.* no overlap), the loss falls back to the smooth  $\ell_1$  loss between the branch output and ground-truth.

$$\mathbf{L}(\mathbf{D}, \mathbf{G}) = \begin{cases} -\ln(\text{IoU}(\mathbf{D}, \mathbf{G})), & \text{if } \text{IoU}(\mathbf{D}, \mathbf{G}) > 0 \\ \text{smooth} \ell_1(\mathbf{D}, \mathbf{G}), & \text{otherwise} \end{cases} \quad (10)$$

During inference, for each detected object trajectory in the log snippet, we first apply the box branch to re-estimate the object size and adjust the motion path accordingly. Then, we apply the path branch to the full trajectory in a sliding window fashion. Note that Auto4D is applicable to both static and moving objects. To avoid small motions for static objects, we add a classification output to the pre-trained object detector to determine whether the object is static or not. If it is a static object, we run the path branch only once on the detection with the highest confidence score over the trajectory.

## 4. Experiments

We evaluate the proposed model from two perspectives: efficacy and practical value. First, given noisy object trajectories from an off-the-shelf detector and tracker, we evaluate how much the model improves the trajectory quality. Second, we investigate the annotation quality through iterative refinement with human input in the loop.

Additionally, we perform a number of ablation studies to demonstrate the value in our design decisions. Finally, we provide qualitative results to visualize the benefit of our work.

### 4.1. Dataset and Evaluation Metrics

We collect a large-scale driving dataset (dubbed Car4D) with LiDAR sensor (Velodyne HDL-64E) data. We trim 5487 scenes that span 25 seconds each, and annotate the vehicles in the scenes with 4D object labels (3D bounding boxes with consistent identifiers across time) using human labelers. We create a train/val/test split with 4662/336/489 scenes each. Since our model is meant to generate automatic ground truth, we consider its ability to generate annotations that are sufficiently close to human annotated results such that they can directly be used for training perception models. To this end, we compute two main metrics: *box agreement* and *corner agreement*.

The *box agreement* measures the quality of a bounding box as a whole. In particular, we adopt intersection-over-union (IoU) which is the commonly used metric in object detection in 2D BEV space. To evaluate the rate of success of our method at producing acceptable automatic labels at different quality requirements, we compute the percentages of boxes whose IoUs with human labels are greater than various thresholds ranging from 0.5 to 0.9. Note that while common benchmarks such as [11] focus on IoU thresholds of 0.7, here we place higher value on high quality boxes and focus on IoU thresholds of 0.8 and 0.9.

In addition, we observe that the number of clicks a human annotator must input to correct labels is directly related to the number of misaligned corners within a bounding box. Hence, we propose the *corner agreement* metric which computes the percentage of box corners with  $\ell_2$  distance to

Method	Box Recall					Corner Recall		
	$\geq 0.5$ IoU	$\geq 0.6$ IoU	$\geq 0.7$ IoU	$\geq 0.8$ IoU	$\geq 0.9$ IoU	$\leq 20$ cm	$\leq 10$ cm	$\leq 5$ cm
Online detector + discrete tracker	98.8%	97.5%	94.0%	82.2%	40.6%	60.8%	31.5%	10.9%
Offline detector + discrete tracker	99.0%	97.9%	94.7%	83.3%	41.5%	61.4%	32.0%	11.2%
Offline detector + disc. & cont. tracker	<b>99.5%</b>	<b>98.4%</b>	95.0%	82.9%	41.3%	61.5%	32.0%	11.3%
Auto4D (local)	98.9%	97.7%	94.8%	85.4%	49.0%	66.4%	35.6%	12.7%
Auto4D (local + global)	99.0%	98.0%	<b>95.6%</b>	<b>87.9%</b>	<b>55.3%</b>	<b>69.7%</b>	<b>39.6%</b>	<b>15.0%</b>

Table 1. **Evaluation of 4D object refinement on Car4D test set.** Our approaches are initialized with object trajectories from the online detector and discrete tracker.

the ground-truth smaller than 20, 10, and 5 centimeters respectively.

Note that our evaluation metrics do not take into account false positives, false negatives or tracking errors, as these are not the main focus of the proposed method. In practice, these errors can be quickly corrected by annotators when we deploy the model in a human-in-the-loop setting [5, 1].

## 4.2. 4D Object Refinement

**Baselines:** Our first baseline is **online detector + discrete tracker**, which is a well researched option for obtaining 4D object trajectories. In particular, we follow HDNET [38] and train a bird-eye-view (BEV) vehicle detector that takes LiDAR data and map information as input. For richer object observation and more accurate motion estimation, we aggregate multi-sweep LiDAR point clouds from a 0.5 second history following FAF [23]. We adopt a distance based tracker similar to that used in FAF [23], where we first propagate the detection from previous frame to current according to its motion estimate, and then perform Hungarian matching [15] based on its center distances (in BEV space) with current frame’s detections. We also memorize motion predictions of unassociated objects (up to 0.5 seconds) to handle short-term occlusion, which happens quite often in self-driving scenarios. Note that our approach is also initialized with this simplest baseline. Despite given online detections as input, our approach refines them in an offline manner by exploiting both past and future information. In comparison, the second baseline extends the first one with an **offline detector**, where both past and future 0.5 second LiDAR sweeps are taken as input. In addition to offline size re-estimation, our approach also smooths the motion path. Finally, the third baseline extends the second one with a **discrete and continuous tracker**, where the continuous refinement is implemented with Kalman filtering [14].

**Evaluation Results:** We show the evaluation results in Table 1, where we compare different methods with

box/corner recalls at different IoU/distance thresholds. By comparing the baselines, we see that exploiting future information (offline detector) helps generate better boxes with richer object observations (with views from different angles), which is revealed by the around 1% absolute increase at 0.8 and 0.9 IoU. Applying filtering to smooth the trajectory (continuous tracker) also helps as temporal consistency is improved. In practice, the trajectory smoothing provides a reasonable estimate of the object pose when the observation is sparse due to distance or occlusion. Therefore, we observe the largest gains at looser IoU tolerances of 0.5 and 0.6.

While the two baselines show incremental improvements only, our learning based approach is able to achieve a remarkable performance boost. Specifically, with box branch alone that re-estimates the object size by aggregating full-trajectory information, we see 8.4% absolute increase in box recall at 0.9 IoU, and 5.6% gain in corner recall at 20 cm. When path branch is applied to refine the motion path, we further improve the aforementioned box recall by 6.3% and corner recall by 3.3%. Applying the two branches together, we improve the box recall at 0.9 IoU from 40.6% to 55.3%. This implies that our model has the potential to save 24.7% of annotation effort if a *box agreement* of 0.9 is acceptable as a replacement to human annotated ground truth, while the savings rise to 32.0% at a lower threshold of 0.8. Note that other empirical studies [5] demonstrated a 85% agreement between human annotators in settings such as segmentation labeling which is arguably easier and less ambiguous, thus putting an upper bound of achievable savings.

## 4.3. Ablation Study

We conduct several ablation studies to better understand how the model works. All experiments are evaluated on the Car4D validation set with the same initial trajectories.

Model	Objects	0.8IoU	0.9IoU	20cm	10cm
Local	Static	<b>+4.8%</b>	<b>+12.1%</b>	<b>+8.2%</b>	<b>+6.4%</b>
	Dynamic	+2.4%	+7.7%	+4.7%	+2.5%
Local + Global	Static	+2.6%	+4.9%	+2.9%	+3.9%
	Dynamic	<b>+4.4%</b>	<b>+7.9%</b>	<b>+4.4%</b>	<b>+4.7%</b>

Table 2. **Ablation on static versus dynamic objects.** We show metric changes in absolute values brought by applying local and global branches one by one.

Local	Global	0.8IoU	0.9IoU	20cm	10cm
✗	✓	+2.8%	+3.7%	+2.1%	+1.4%
center-align	✗	+1.5%	+3.5%	+1.4%	-0.8%
corner-align	✗	+3.3%	+9.5%	+6.3%	+4.4%
✓	✓	<b>+6.8%</b>	<b>+16.3%</b>	<b>+9.9%</b>	<b>+8.7%</b>

Table 3. **Ablation on object size re-estimation.**

**Static versus Dynamic Objects:** We first isolate at our model performance on static and dynamic objects respectively, and show the results in Table 2. When we apply box branch to the initial trajectories, we see much more significant improvements on static objects than dynamic objects. This is because for static objects we are more likely to get observations from multiple views than dynamic objects, and therefore the size estimation from temporally aggregated observation will be more accurate. Moreover, the aggregation of LiDAR points in the world coordinate system has relatively little noise, leading to a clean point cloud. When the path branch is applied, the situation is reversed. Here, we observe more gains on dynamic objects than static objects, as the path branch is designed to exploit both LiDAR observation and temporal motion cues to refine the motion path.

**Object Size:** One key idea of our approach is to separate object size from the motion path, as the size stays the same but the locations do not. As model optimizes the two factors separately, we explore different ways of combining them. In Table 3 we first create a baseline model (*i.e.* path branch only) that jointly optimizes size and location at frame level (like an object detector), and this baseline achieves around 2% gain in all metrics. In contrast, our full model that has both box and path branches can achieve up to 16% absolute gain in object recall at 0.9 IoU. The significant gain comes from two aspects. First, the re-estimated object size becomes a constant along the trajectory. Second, better size leads to better motion path if used properly. In terms of the second aspect, we further compare two different strategies to relate object size with its location, namely center-align and corner-align. We discover that aligning the bounding

	0.8IoU	0.9IoU	20cm	10cm
w/o localization	+4.8%	+12.1%	+8.2%	+6.4%
w/ localization	<b>+4.9%</b>	<b>+12.9%</b>	<b>+9.5%</b>	<b>+9.1%</b>

Table 4. **Ablation on using localization prior for the box branch.** We show relative gains on static objects only.

	0.8IoU	0.9IoU	20cm	10cm
Iter 1	+6.8%	+16.3%	+9.9%	+8.7%
Iter 2	+0.0%	<b>+1.0%</b>	<b>+0.7%</b>	<b>+0.7%</b>

Table 5. **Evaluation results under the annotator-in-the-loop setting.** After one iteration of label refinement, we fix the tracking fragmentations by linking object trajectories belong to the same instance together. Given this external feedback, our model performs second iteration of trajectory refinement.

box to the closest observed corner results in higher performance. While the center-align scheme produces modest improvements in the IoU metric, it decreases the level of corner agreement. On the other hand, corner-align provides significant improvements in both metrics. This validates our intuition.

**Exploit Localization for Static Objects:** While the path branch of our model relies on ego-vehicle localization to reason about object motion in the world coordinate system, the box branch does not directly exploit such information as it aggregates evidences in the object coordinate system. This has the benefit of a unified model for both static and dynamic objects. However, to estimate the size of static objects, we can leverage the ego-vehicle’s localization to directly aggregate the LiDAR sweeps into a clean shape in the world coordinate system without the effects of noisy pose estimates. This may potentially produce better object reconstruction. We compare reasoning in box coordinates and world coordinates for static object size estimation in Table 4, and show that exploiting the ego-vehicle localization prior (which has centimeter-level accuracy in Car4D dataset) offers slightly better performance. However, the gain is quite incremental, showing that our box branch is capable of recovering accurate object size from noisy object reconstructions.

#### 4.4. Annotator-in-the-Loop

As a refinement model, our approach can naturally be integrated into the annotator-in-the-loop framework such as that used by [5]. At each iteration, the annotator corrects the errors in the refined labels, and the modified labels are further fed to our model for the next round of refinement. Here we mimic this process by automatically correcting the tracking fragmentation errors. To be more specific, after the

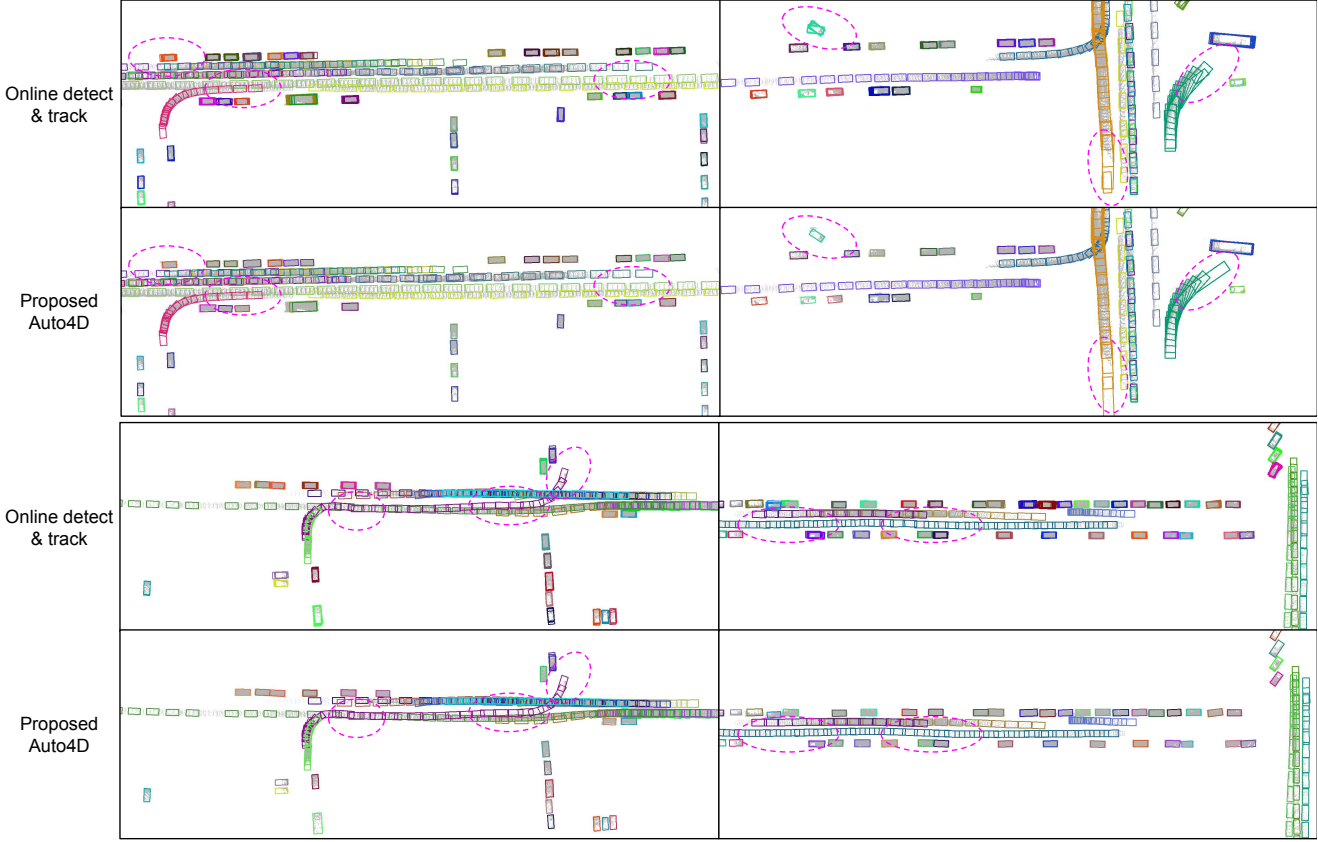


Figure 3. **Qualitative results of the online detection & tracking results versus Auto4D results.** We draw detected object trajectories (color) together with their enclosing point clouds (grey) in the world coordinates. We draw bounding boxes at 2 Hz to avoid clutter. Significant improvements are highlighted with pink circles.

first iteration, we automatically link trajectories together if they belong to the same object instance (which in practice can be as simple as two clicks from the annotator). The resulting longer trajectories are then fed to the model again for the second round of refinement. Note that the two refinement iterations share the same model. From the results in Table 5 we see that our model is able to incorporate such minimal human feedback to further improve the label quality.

#### 4.5. Qualitative Results

In Figure 6 we show some qualitative results of the proposed Auto4D in comparison with the initialization object trajectories from the state-of-the-art online detector and tracker. In general we find that our approach produces more accurate bounding boxes for static objects free from small jitters. For moving objects, thanks to the fixed size constraint, we are able to correctly estimate the object’s location even when it is far away from the ego-car and the observation is very sparse. Overall the generated trajectories tend to be smoother and more natural. We refer readers to

the supplementary materials for more qualitative results.

## 5. Conclusion

While previous automatic labeling methods mainly focus on generating 2D or 3D labels at frame level, in this paper we take one step forward by using extended temporal information to produce smooth and consistent object trajectories over time. Towards this goal we propose to decompose the 4D label into two components: object size and motion path. The object size is fixed across time, while the motion path describes how the object pose (center position and orientation) changes over time. Our model works by taking imperfect but cheap object trajectories (*e.g.* from off-the-shelf detector and tracker) as input, and learns to refine them (size & path) by exploiting spatial-temporal information over the full trajectory. We validate the approach on a large-scale driving dataset with high-quality annotations, and show significant improvement over various detector baselines and model-based tracking baseline. Because our model follows the refinement paradigm, our model is also suitable for the annotator-in-the-loop framework. In

the future, we plan to extend the approach to incorporate additional information sources such as camera images.

## References

[1] David Acuna, Huan Ling, Amlan Kar, and Sanja Fidler. Efficient Annotation of Segmentation Datasets with Polygon-RNN++. In *CVPR*, 2018. 1, 2, 6

[2] Holger Caesar, Varun Bankiti, Alex H Lang, Sourabh Vora, Venice Erin Liong, Qiang Xu, Anush Krishnan, Yu Pan, Giacarlo Baldan, and Oscar Beijbom. nuscenes: A multimodal dataset for autonomous driving. In *CVPR*, 2020. 2

[3] Sergio Casas, Cole Gulino, Simon Suo, Katie Luo, Renjie Liao, and Raquel Urtasun. Implicit latent variable model for scene-consistent motion forecasting. In *ECCV*, 2020. 1

[4] Sergio Casas, Wenjie Luo, and Raquel Urtasun. Intentnet: Learning to predict intention from raw sensor data. In *CoRL*, 2018. 5

[5] Lluis Castrejon, Kaustav Kundu, Raquel Urtasun, and Sanja Fidler. Annotating Object Instances with a Polygon-RNN. In *CVPR*, 2017. 2, 6, 7

[6] Yuning Chai, Benjamin Sapp, Mayank Bansal, and Dragomir Anguelov. Multipath: Multiple probabilistic anchor trajectory hypotheses for behavior prediction. In *CoRL*, 2019. 1

[7] Xiaozhi Chen, Huimin Ma, Ji Wan, Bo Li, and Tian Xia. Multi-view 3d object detection network for autonomous driving. In *CVPR*, 2017. 2

[8] Martin Engelcke, Dushyant Rao, Dominic Zeng Wang, Chi Hay Tong, and Ingmar Posner. Vote3deep: Fast object detection in 3d point clouds using efficient convolutional neural networks. In *ICRA*, 2017. 2

[9] Christoph Feichtenhofer, Axel Pinz, and Andrew Zisserman. Detect to track and track to detect. In *ICCV*, 2017. 2

[10] Davi Frossard, Simon Suo, Sergio Casas, James Tu, Rui Hu, and Raquel Urtasun. Strobe: Streaming object detection from lidar packets. In *CoRL*, 2020. 2

[11] Andreas Geiger, Philip Lenz, and Raquel Urtasun. Are we ready for autonomous driving? the kitti vision benchmark suite. In *CVPR*, 2012. 2, 5

[12] Chenhang He, Hui Zeng, Jianqiang Huang, Xian-Sheng Hua, and Lei Zhang. Structure aware single-stage 3d object detection from point cloud. In *CVPR*, 2020. 1

[13] Hou-Ning Hu, Qi-Zhi Cai, Dequan Wang, Ji Lin, Min Sun, Philipp Krahenbuhl, Trevor Darrell, and Fisher Yu. Joint Monocular 3D Vehicle Detection and Tracking. In *ICCV*, 2019. 2

[14] Rudolph Emil Kalman. A new approach to linear filtering and prediction problems. 1960. 6

[15] Harold W Kuhn. The hungarian method for the assignment problem. *Naval research logistics quarterly*, 2(1-2):83–97, 1955. 6

[16] Alex H Lang, Sourabh Vora, Holger Caesar, Lubing Zhou, Jiong Yang, and Oscar Beijbom. Pointpillars: Fast encoders for object detection from point clouds. In *CVPR*, 2019. 2

[17] Jungwook Lee, Sean Walsh, Ali Harakeh, and Steven L Waslander. Leveraging pre-trained 3d object detection models for fast ground truth generation. In *2018 21st International Conference on Intelligent Transportation Systems (ITSC)*, 2018. 2

[18] Bo Li. 3d fully convolutional network for vehicle detection in point cloud. In *IROS*, 2017. 2

[19] Bo Li, Tianlei Zhang, and Tian Xia. Vehicle detection from 3d lidar using fully convolutional network. In *RSS*, 2016. 2

[20] Ming Liang, Bin Yang, Wenyuan Zeng, Yun Chen, Rui Hu, Sergio Casas, and Raquel Urtasun. PnPNet: End-to-End Perception and Prediction with Tracking in the Loop. In *CVPR*, 2020. 1, 2

[21] Tsung-Yi Lin, Piotr Dollár, Ross Girshick, Kaiming He, Bharath Hariharan, and Serge Belongie. Feature pyramid networks for object detection. In *CVPR*, 2017. 10

[22] Huan Ling, Jun Gao, Amlan Kar, Wenzheng Chen, and Sanja Fidler. Fast Interactive Object Annotation With Curve-GCN. In *CVPR*, 2019. 2

[23] Wenjie Luo, Bin Yang, and Raquel Urtasun. Fast and furious: Real time end-to-end 3d detection, tracking and motion forecasting with a single convolutional net. In *CVPR*, 2018. 2, 6

[24] Qinghao Meng, Wenguan Wang, Tianfei Zhou, Jianbing Shen, Luc Van Gool, and Dengxin Dai. Weakly supervised 3d object detection from lidar point cloud. In *ECCV*, 2020. 2

[25] Gregory P Meyer, Ankit Laddha, Eric Kee, Carlos Valdespi-Gonzalez, and Carl K Wellington. Lasernet: An efficient probabilistic 3d object detector for autonomous driving. In *CVPR*, 2019. 1, 2

[26] Anton Milan, Stefan Roth, and Konrad Schindler. Continuous energy minimization for multitarget tracking. In *PAMI*, 2014. 1, 2

[27] Charles R Qi, Wei Liu, Chenxia Wu, Hao Su, and Leonidas J Guibas. Frustum pointnets for 3d object detection from rgbd data. In *CVPR*, 2018. 2

[28] Olaf Ronneberger, Philipp Fischer, and Thomas Brox. U-net: Convolutional networks for biomedical image segmentation. In *International Conference on Medical image computing and computer-assisted intervention*, 2015. 5

[29] Olaf Ronneberger, Philipp Fischer, and Thomas Brox. U-net: Convolutional networks for biomedical image segmentation. In *International Conference on Medical image computing and computer-assisted intervention*, 2015. 11

[30] Shaoshuai Shi, Chaoxu Guo, Li Jiang, Zhe Wang, Jianping Shi, Xiaogang Wang, and Hongsheng Li. Pv-rcnn: Point-voxel feature set abstraction for 3d object detection. In *CVPR*, 2020. 1, 2

[31] Weijing Shi and Ragunathan Rajkumar. Point-gnn: Graph neural network for 3d object detection in a point cloud. In *CVPR*, 2020. 2

[32] Christian Szegedy, Sergey Ioffe, Vincent Vanhoucke, and Alex Alemi. Inception-v4, inception-resnet and the impact of residual connections on learning. In *AAAI*, 2017. 10

[33] Sean Walsh, Jason Ku, Alex D Pon, and Steven L Waslander. Leveraging temporal data for automatic labelling of static vehicles. In *17th Conference on Computer and Robot Vision (CRV)*, 2020. 1, 2

- [34] Bernie Wang, Virginia Wu, Bichen Wu, and Kurt Keutzer. Latte: accelerating lidar point cloud annotation via sensor fusion, one-click annotation, and tracking. In *IEEE Intelligent Transportation Systems Conference (ITSC)*, 2019. [2](#)
- [35] Shiyao Wang, Yucong Zhou, Junjie Yan, and Zhidong Deng. Fully motion-aware network for video object detection. In *ECCV*, 2018. [2](#)
- [36] Xinshuo Weng, Jiaren Wang, David Held, and Kris Kitani. 3d multi-object tracking: A baseline and new evaluation metrics. *IROS*, 2020. [1](#)
- [37] Xinshuo Weng, Jianren Wang, David Held, and Kris Kitani. 3d multi-object tracking: A baseline and new evaluation metrics. In *IROS*, 2020. [3](#)
- [38] Bin Yang, Ming Liang, and Raquel Urtasun. Hdnet: Exploiting hd maps for 3d object detection. In *CoRL*, 2018. [1](#), [2](#), [3](#), [6](#)
- [39] Bin Yang, Wenjie Luo, and Raquel Urtasun. Pixor: Real-time 3d object detection from point clouds. In *CVPR*, 2018. [2](#)
- [40] Zetong Yang, Yanan Sun, Shu Liu, and Jiaya Jia. 3dssd: Point-based 3d single stage object detector. In *CVPR*, 2020. [1](#), [2](#)
- [41] Zetong Yang, Yanan Sun, Shu Liu, Xiaoyong Shen, and Jiaya Jia. Std: Sparse-to-dense 3d object detector for point cloud. In *ICCV*, 2019. [1](#), [2](#)
- [42] Tianwei Yin, Xingyi Zhou, and Philipp Krähenbühl. Center-based 3d object detection and tracking. *arXiv preprint arXiv:2006.11275*, 2020. [2](#)
- [43] Sergey Zakharov, Wadim Kehl, Arjun Bhargava, and Adrien Gaidon. Autolabeling 3d objects with differentiable rendering of sdf shape priors. In *CVPR*, 2020. [2](#)
- [44] Yin Zhou and Oncel Tuzel. Voxelnet: End-to-end learning for point cloud based 3d object detection. In *CVPR*, 2018. [2](#)
- [45] Xizhou Zhu, Yujie Wang, Jifeng Dai, Lu Yuan, and Yichen Wei. Flow-guided feature aggregation for video object detection. In *ICCV*, 2017. [2](#)

## Appendix

### A. Implementation Details

#### A1. Object Size Branch

**LiDAR BEV Representation:** Given an initial trajectory consisting of a sequence of detection bounding boxes, we define the aggregation box coordinate frame with reference to the detection box with the highest confidence score. All the object observation points are aggregated through time in this box coordinate frame. We voxelize the aggregated points (regardless of time) into a 3D occupancy grid. We define each LiDAR point feature to be 1, and compute the voxel feature by summing all enclosing point features weighted by their relative positions to the voxel center. We treat height slices as feature channels as therefore consider the voxel grid as LiDAR bird-eye-view (BEV) representation. The voxel size is 5 cm in X and Y axes, and 10 cm in Z axis. The volume of the voxel grid is [-12, 12] meters  $\times$

[-4, 4] meters  $\times$  [-0.2, 3.0] meters, which covers the sizes of more than 99% objects in our training set.

**Encoder Network:** The encoder network architecture is shown in Figure 4. To be more specific, we first use three Conv2D layers to down-sample the input BEV representation by 4. We then apply a cross-scale module sequentially for three times. The cross-scale module is inspired by the Inception block with residual connections [32]. The difference is that features are spanned at multiple scales (3 in our case), and each scale receives information from other scales. This leads to a better trade-off between accuracy and speed. After three cross-scale modules, we use a feature pyramid network [21] to combine multi-scale features, followed with 4 Conv2D layers each with 256 feature channels. The encoder network outputs a BEV feature map with a feature channel size of 256. The size of the feature map is 16 times smaller compared with the original input, meaning that the stride at the output feature map is 0.8 m.

**Decoder Network:** We simply extract the center feature in box coordinate frame to decode the object size. Specifically, we use bilinear interpolation to extract the center feature from the encoder output feature map, and apply an additional Linear layer to predict the object size, center offset, and orientation. During training we use all outputs to optimize for the IoU loss, during testing we take object size output only.

### A2. Motion Path Branch

**LiDAR BEV Representation:** The motion path branch operates on trajectories of different length in a sliding window fashion. In practice, we define the sliding window to be 1 second, which contains 0.5 s in the past and 0.5 s in the future. The stride of the sliding window is one frame (*i.e.*, 0.1 s), meaning that for each sliding window we exploit 1 second temporal information to refine the object pose at the center frame. The global coordinate frame is also centered and rotated with regard to the detection box at the center frame. We use the similar BEV representation as in the object size branch, except that we stack multi-sweep LiDAR point clouds along the channel dimension. To account for object motion, the size of the voxel grid is [-24, 24] m  $\times$  [-8, 8] m  $\times$  [-0.2, 3.0] m. We use a voxel size of 0.1 m in X, Y and Z axes.

**Encoder Network:** The architecture of the encoder network is almost the same as the one in object size branch 4. The only modification is the first three Conv2D layers. Their numbers of channels are enlarged to 120, 96, 96 to account for higher dimension input. Also, the first Conv2D layer is GroupConv with the number of groups equal to the number of input LiDAR sweeps to save computation.

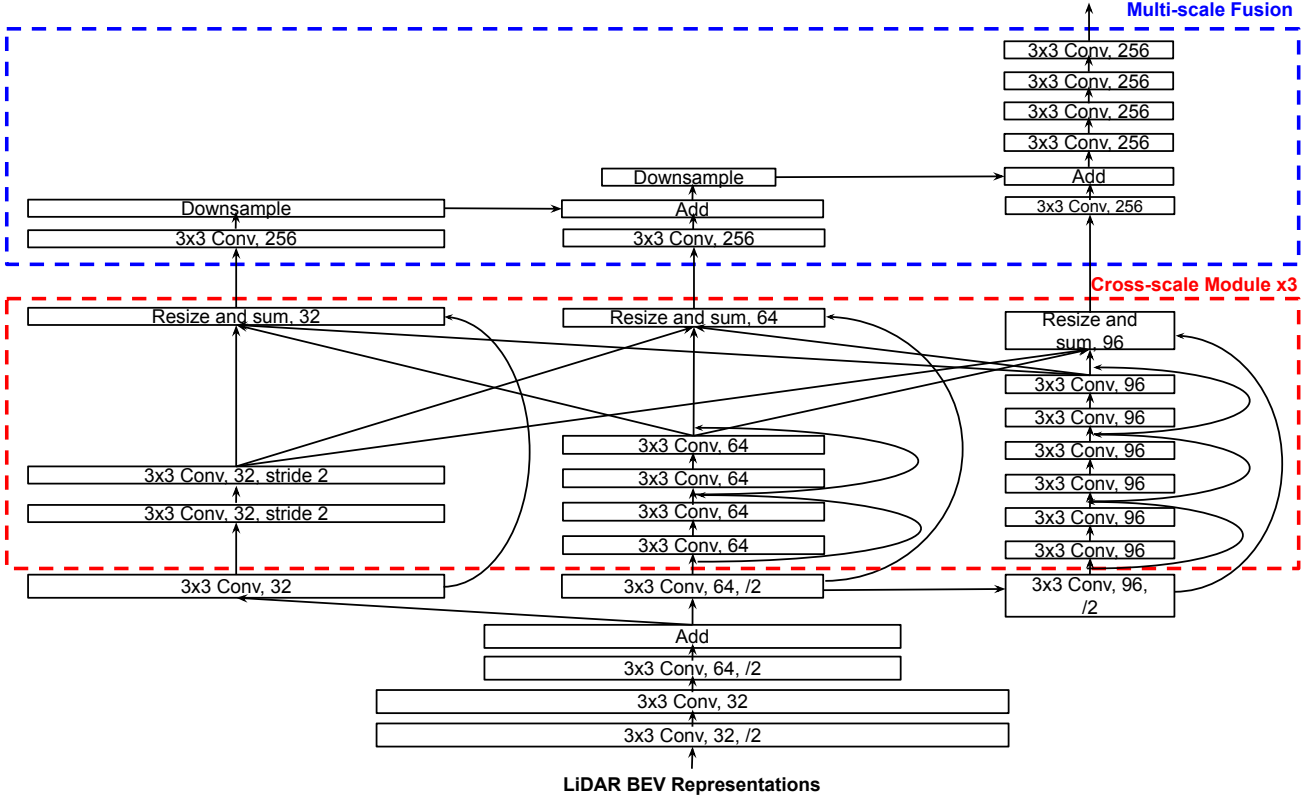


Figure 4. Encoder network architecture.

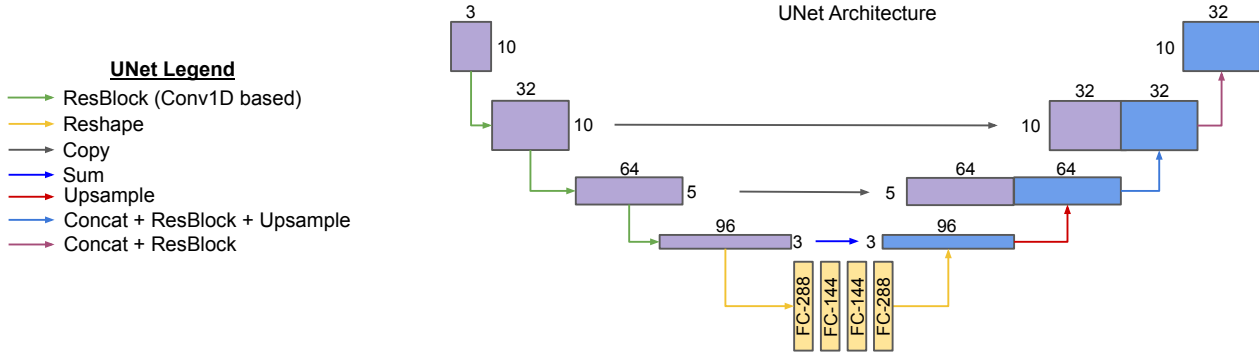


Figure 5. UNet architecture.

We also explicitly compute the motion feature of the path with a Conv1D based UNet [29], whose architecture is shown in Figure 5. We choose UNet to extract temporal features for its efficiency in computation and effectiveness in multi-scale feature learning.

**Decoder Network:** We extract center position observation feature from the 2D encoder feature map, and center frame motion feature from the 1D UNet feature map. We use a MLP to reshape both features to the same dimension and add them together for feature fusion. Lastly we use an

other Linear layer to predict the object pose refinement.

## B. More Qualitative Results

In Figure 6 we show detection-wise results of how our approach produces more accurate boxes compared with the initial detections. From the results we see that online LiDAR based object detectors often have difficulty properly estimate the full extent of the object due to partial observation. Our approach, in contrast, addresses this by exploiting the full trajectory observations.

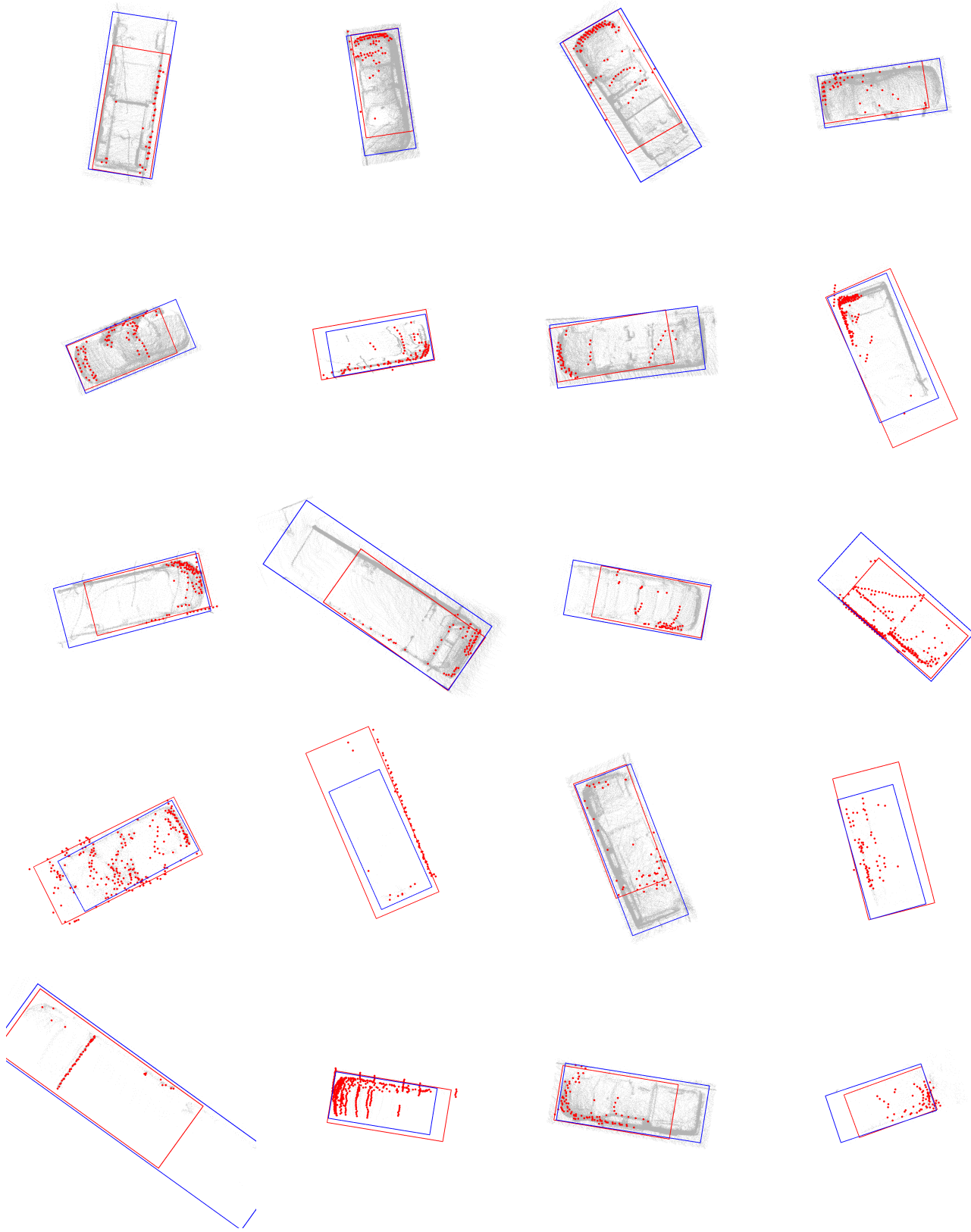


Figure 6. Qualitative comparison of our refined detections (in blue) and the initial detections (in red). We show examples of parked vehicles only. We draw aggregated LiDAR points in red, and single-sweep LiDAR points corresponding to the initial detection timestamp in red.